scientific reports

Check for updates

OPEN

Evaluation of cellular water exchange in a mouse glioma model using dynamic contrast-enhanced MRI with two flip angles

Karl Kiser[1]✉, Jin Zhang[1], Ayesha Bharadwaj Das[1], James A. Tranos[2], Youssef Zaim Wadghiri[2] & Sungheon Gene Kim[1]

This manuscript aims to evaluate the robustness and significance of the water efflux rate constant (k_{io}) parameter estimated using the two flip-angle Dynamic Contrast-Enhanced (DCE) MRI approach with a murine glioblastoma model at 7 T. The repeatability of contrast kinetic parameters and k_{io} measurement was assessed by a test–retest experiment (n = 7). The association of k_{io} with cellular metabolism was investigated through DCE-MRI and FDG-PET experiments (n = 7). Tumor response to a combination therapy of bevacizumab and fluorouracil (5FU) monitored by contrast kinetic parameters and k_{io} (n = 10). Test–retest experiments demonstrated compartmental volume fractions (v_e and v_p) remained consistent between scans while the vascular functional measures (F_p and PS) and k_{io} showed noticeable changes, most likely due to physiological changes of the tumor. The standardized uptake value (SUV) of tumors has a linear correlation with k_{io} ($R^2 = 0.547$), a positive correlation with F_p ($R^2 = 0.504$), and weak correlations with v_e ($R^2 = 0.150$), v_p ($R^2 = 0.077$), PS ($R^2 = 0.117$), K^{trans} ($R^2 = 0.088$) and whole tumor volume ($R^2 = 0.174$). In the treatment study, the k_{io} of the treated group was significantly lower than the control group one day after bevacizumab treatment and decreased significantly after 5FU treatment compared to the baseline. This study results support the feasibility of measuring k_{io} using the two flip-angle DCE-MRI approach in cancer imaging.

The water efflux rate constant (k_{io}) is a parameter of interest for oncology studies since cellular water exchange may reflect pathophysiological conditions of the cancer cells[1]. Cellular-interstitial water exchange may be a sensitive indicator of cellular energy turnover, as the water exchange depends on cell membrane ion-pump activities, a measure of glycolysis and mitochondrial respiration[2,3]. Increased expression of transmembrane water channels, aquaporins (AQPs), and subsequent increase of cell membrane permeability are associated with angiogenesis, proliferation and metastatic potential in cancer[4]. Estimation of k_{io} from pharmacokinetic modeling of dynamic contrast-enhanced (DCE) MRI has shown sensitivity to these different mechanisms of cellular water exchange[1]. Furthermore, several cancer studies have demonstrated the feasibility of using k_{io} for tumor selection and grading[5–7] and predicting treatment response[1,8–10] including long term survivability[11].

However, achieving accurate and reliable estimation of k_{io} from DCE-MRI data has proven to be non-trivial due to the sensitivity of k_{io} estimation to various experimental conditions, such as MRI scan parameters, arterial input function (AIF) and selection of contrast kinetic models[12–14]. It was also reported that the degree of water exchange effect on DCE-MRI data depends on scan protocols including the flip angle[12,15]. This flip angle dependency was leveraged in a previous study[16] to improve the accuracy of k_{io} estimation by actively encoding the water exchange effect in the washout phase of the DCE scan with a series of multiple flip angles, i.e., with different sensitivities to cellular water exchange. As the weighting of the water exchange effect changes with the different flip angle segments, one set of contrast kinetic parameters cannot adequately model the data without including the k_{io} term.

The present study aims to evaluate the robustness and significance of the k_{io} parameter estimated using the two flip-angle DCE-MRI approach in GL261 murine glioma model. The repeatability of contrast kinetic parameter measurement and k_{io} was assessed by a test–retest DCE-MRI experiment. The association of k_{io} with cellular metabolism was investigated through consecutive DCE-MRI and ^{18}F-fluorodeoxyglucose (FDG)—Positron

[1]Department of Radiology, Weill Cornell Medical College, 1300 York Avenue, New York, NY 10065, WMC Box 141, USA. [2]Center for Biomedical Imaging (CBI), Center for Advanced Imaging Innovation and Research (CAI2R), Department of Radiology, NYU Grossman School of Medicine, New York, NY, USA. ✉email: karl.j.kiser@gmail.com

Emission Tomography (PET) scans. Finally, we assessed the feasibility of k_{io} in evaluating tumor progression and response to chemotherapy.

Methods

Animal model. Six to eight-week-old C57BL6 mice ($n = 24$; female) with GL261 mouse glioma models were included in this study for repeatability measurement (n = 7), comparison with FDG-PET (n = 7), and assessment of treatment response (n = 10), as described below in detail. For this study to assess the feasibility of using the proposed two-flip angle DCE-MRI method, no power calculation was used to determine the sample size. The mice were inoculated with 1×10^5 GL261 mouse glioma cells suspended in 4μL of phosphate buffered saline (PBS) solution using a Hamilton syringe for stereotactic intracranial injection into the subcortex (2.5 mm depth). The inclusion criterion was to have successful tumor growth observed by MRI between day 15 and 26 after tumor inoculation. The exclusion criterion was to have any sign of pain and distress. All the mice included in this study meet these criteria. All animals were treated in strict accordance with the National Institutes of Health Guide for the Care and Use of Laboratory Animals, and this study was approved by the institutional animal care of use committees (IACUC) at Weill Cornell Medical College and New York University School of Medicine and reported in accordance with ARRIVE guidelines.

DCE-MRI data acquisition. MRI scans were performed on a Bruker 7 T micro-MRI system equipped with an 80-mm transmit-only birdcage coil and a ^{1}H four-channel phased array cryogenically cooled receive-only mouse brain MRI coil. DCE-MRI image acquisition was performed using the 3D ultra-short echo-time (UTE) pulse sequence ($TR = 4$ ms and $TE = 0.028$ ms) with 3D Golden angle Radial Sparse Parallel (GRASP) MRI method to achieve an isotropic spatial resolution and to minimize the T_2^* effect. The pulse sequence was continuously run to acquire 154,080 spokes for 10 min and 13 s[16]. The two flip-angle DCE-MRI method was implemented by using a series of three flip angle segments (8°-25°-8°) with 51,360 spokes per flip angle segment (image matrix size = 128 × 128 × 128, field of view = 20 × 20 × 20 mm^3, and the spatial resolution = 0.156 × 0.156 × 0.156 mm^3). The segments with a low flip angle (8°) are expected to have larger effects of the cellular-interstitial water exchange than the one with a high flip angle (25°)[16]. A bolus of gadolinium-based contrast agent (GBCA) in saline at the dose of 0.1 mmol/kg was injected through a tail vein catheter, starting 60 s after the start of data acquisition; gadoxetate disodium (Eovist, Bayer) was used for the repeatability measurement and gadobutrol (Gadavist, Bayer) for comparison with FDG-PET and assessment of treatment response, assuming these two GBCAs work similarly as non-specific contrast agents in tumor. Prior to each DCE-MRI experiment, a 3D T_1 map with the same isotropic high resolution was obtained using the same 3D-UTE-GRASP sequence with variable flip angles (8°-2°-12°, 12,776 spokes for each flip angle, total acquisition time = 153 s)[16].

DCE-MRI data analysis. Image reconstruction was conducted using the joint compressed sensing and parallel imaging reconstruction method based on the 3D-UTE-GRASP algorithm[17] in order to achieve a temporal frame resolution $T = 5$ s/frame. Arterial input function (AIF) was obtained from the early enhancing vascular voxels following the Principal Component Analysis (PCA) method used in our previous study[18]. The T_1-weighted images were used to manually segment tumors. The independently measured pre-contrast T_1 map was used to convert the DCE-MRI signal intensity data to GBCA concentration data with the assumption of the tissue relaxivity ($r_1 = 5.1$ s^{-1} mmol^{-1} for gadoxetate and 3.3 s^{-1} mmol^{-1} for gadobutrol) and a homogeneous radiofrequency transmit field for the volume coil (i.e., $B_1^+ = 1$). Pharmacokinetic model analysis was carried out for the whole tumor with the Two Compartment Exchange Model (TCM)[19] for GBCA combined with the Three Site Two Exchange Model (3S2X)[15,20,21] for water exchange in order to estimate five parameters: interstitial space volume fraction (v_e), vascular space volume fraction (v_p), blood flow (F_p), permeability surface area product (PS), and water efflux rate constant (k_{io}). Transfer constant (K^{trans}) was calculated from PS and F_p ($K^{trans} = [1\text{-}exp(-PS/F_p)]\ Fp$). In addition to k_{io} which reflects the efflux rate constant from the intracellular compartment, we also included a transcytolemmal exchange rate constant defined as $k_{ex} = k_{io}/v_e = k_{oi}/v_i$ ($i.e.\ \tau_{ex} = v_e\tau_i = v_i\tau_e$), which takes into account the compartmental volume fractions[22–24]. We assumed that the water fraction f_w is 1 in all compartments for simplicity; while the conventional assumption is $f_w = 0.8$ for the normal brain, it is not trivial to find appropriate f_w values for the intra- and extracellular compartments in various locations of heterogeneous tumors like the ones included in this study.

Test–retest repeatability. The repeatability of contrast kinetic parameter and k_{io} estimation was measured in the C57BL6 mice with GL261 intracranial tumors (n = 7) between day 15 and day 26 after tumor inoculation in the brain. For each mouse, the DCE-MRI scan with two flip angles was conducted twice with an interval of 30 min between the end of the first DCE-MRI scan and the beginning of the second scan with the T_1 mapping followed by the second DCE-MRI. Upon the completion of the first scan, the mouse was moved out of the magnet and then repositioned in the magnet for the second scan. Each DCE-MRI scan included a GBCA injection at the dose of 0.1 mmol/kg. To align the tumor voxels between the first and the second DCE-MRI scans, the images of the second DCE-MRI scan (both T_1 map and DCE-MRI) were registered to the images of the first DCE-MRI by applying rigid body transformation through minimization of the sum of mean squared differences between the two 3D image datasets (Fig. 1).

The contrast kinetic parameters and k_{io} of tumor voxels from the two scans were compared at the voxel level using the Wilcoxon signed rank test. The contrast kinetic parameter and k_{io} maps of the test and re-test scans were also compared in terms of texture features extracted using the open-source Python package PyRadiomics[25]. We included 93 features; First Order Histogram Features (n = 18 features), Gray Level Co-occurrence Matrix (GLCM; n = 24), Gray Level Dependence Matrix (GLDM; n = 14), Gray Level Run Length Matrix (GLRLM; n = 16), Gray

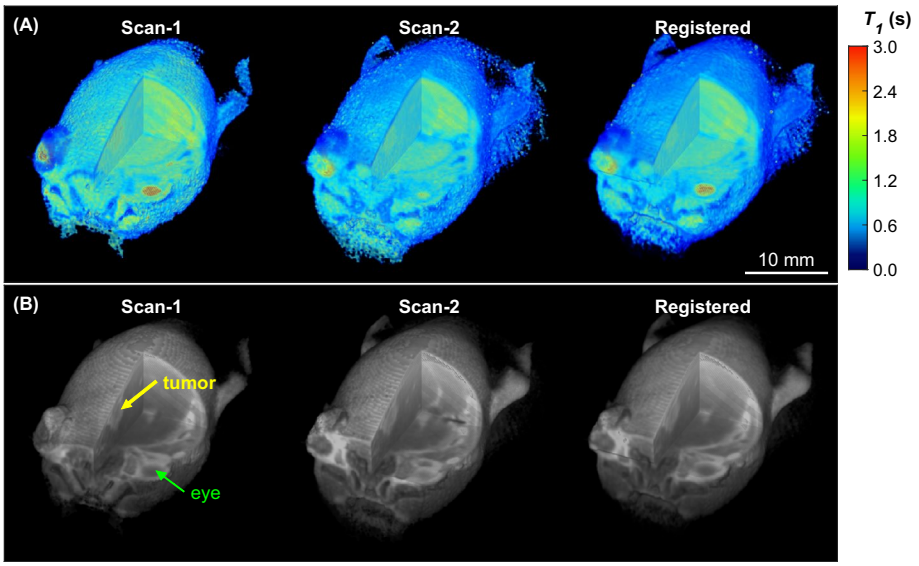

Figure 1. Volume rendered images of the two consecutive DCE-MRI scans of a same mouse with an interval of 30 min. A cutout is made to show the cross-sections through a tumor (yellow arrow) and an eye (green arrow). The images of Scan-2 were registered to those of Scan-1 as shown in the right column. (**A**) 3D T1 map generated from 3D-UTE-GRASP images with three flip angles. (**B**) One of DCE-MR images, reconstructed with a temporal resolution of 5 s/frame, corresponding to 120 s after contrast injection.

Level Size Zone Matrix (GLSZM; n = 16), and Neighboring Gray Tone Difference Matrix (NGTDM; n = 5). In addition to the contrast kinetic parameter and k_{io} maps, the last frame of the DCE-MR images was included as delayed contrast enhanced images for extracting texture features. Discretization of the dynamic ranges of the contrast enhanced images and parameter maps was performed using a fixed bin width determined by the Freedman-Diaconis rule: $W = 2\ (IQR)\ N^{-1/3}$, where IQR is the interquartile range and N is the number of pixels[26]. The default PyRadiomics configuration was used for all other texture feature extraction settings (see http://pyradiomics.readthedocs.io for further information). Statistical analysis of texture feature differences between two images was performed using the paired Student's t-test. To keep the family-wise error rate to 0.05 for each parameter, we used the significance level for a single hypothesis test of 0.0006.

Comparison of DCE-MRI with FDG-PET. Previous studies have shown that the water exchange across the cell plasma membrane is associated with the expression of the ATP-dependent ion channels[2,3]. The goal of this experiment is to assess the association between k_{io} as a measure of transcytolemmal water exchange and FDG uptake as a marker for cellular metabolism. Six to eight-week-old C57BL6 mice ($n = 7$) with GL261 mouse glioma xenograft models were used for this experiment. k_{io} was estimated using the two flip-angle DCE-MRI method. To ensure that the well perfused voxels with sufficient GBCA extravasation were selected for reliable measurement of k_{io}, the top 10% of voxels with the highest signal enhancement ratio were selected for analysis[12,20,27–29]. This selection was used particularly due to low contrast enhancement of the glioma model used in this study (average $K^{trans} < 0.1\ min^{-1}$ for all tumors included for this comparison as shown in Fig. 5). We assumed the k_{io} measured from the most enhancing part of the tumor is representative of the whole tumor for the comparison with the FDG-PET. The DCE-MRI scan was immediately followed by ^{18}F-FDG-PET scan per animal. ^{18}F-FDG PET and computed tomography (CT) scans were performed on an Inveon small-animal hybrid PET/CT scanner (Siemens Medical Solutions). The mice were administered an ^{18}F-FDG bolus (6.45–11.1 MBq/0.1 mL) via tail vein injection. The PET data collected for 5 min after 55 min post injection were used to generate the standardized uptake value (SUV) maps. SUV was calculated as: [decay corrected activity (Bq/mL)]/[animal weight (g)]/[injected dose (Bq)]. Whole tumors were manually segmented from co-registered PET/CT images. Since the low spatial resolution of PET images (1.4 mm isotropic) is not adequate for voxel-level analysis, the mean SUV of the whole tumor was used for the comparison with DCE-MRI.

Assessment of treatment response. Two groups of six to eight-week-old C57BL6 mice ($n = 5$ per group) with GL261 mouse glioma model were used to investigate the feasibility of using the two flip-angle DCE-MRI approach for longitudinal assessment of treatment response. For the treatment group, pre-treatment DCE-MRI (Pre-Tx) was immediately followed by an intraperitoneal (IP) injection of bevacizumab (Avastin, Genentech) at 10 mg/kg. After 24 h, mice were scanned again (Tx-1) and subsequently given an IP injection of fluorouracil (5FU, Fressenius Kabi) at 80 mg/kg. A second dose of 5FU (80 mg/kg) was given after 48 h. Post-treatment DCE-MRI (Tx-2) was conducted 24 h after the second 5FU treatment (i.e. 4 days after the pre-treatment DCE-MRI). The control group was treated with sodium chloride solution (10 ml/kg) and imaged at the same time points as the treatment group (Supplementary Fig. 1). Control and treated groups were randomly selected by a co-author

(SGK) who was blinded to the animal status and images at the selection. Blinding of treatment group was not used in this feasibility study with a small number of animals. We assumed the benefit of blinding would be insignificant since the data collection and analysis were conducted with a same scan protocol and data processing pipeline.

Results

Repeatability. The DCE-MRI scans were successfully conducted twice for a group of mice (n = 7) included in this experiment. In all mice, the whole tumor contrast kinetic parameter maps and k_{io} from the two scans of a same tumor appear similar to each other (Fig. 2). Among the estimated parameters, the volume fraction measures, v_e and v_p, show strong correlation between the two scans (Pearson correlation coefficient r = 0.61 for v_e and 0.70 for v_p) and no significant difference between them (P = 0.375 for v_e and 0.467 for v_p; Wilcoxon signed rank test) (Fig. 3). The vascular parameters, *PS*, F_p, and K^{trans}, appear to be greater in the second scan than in the first scan: 41.8% greater for PS (P = 0.109), 261.5% greater for F_p (P = 0.078), and 43.2% greater for K^{trans} (P = 0.047) in terms of the median values. In contrast, k_{io} values increased between the first and second scan by 45.2% of the median value (P = 0.156). Of the 93 histogram and texture features extracted from the parameter maps, 9 features in k_{io} maps and one feature in v_e and v_p maps were found to be significantly different (Supplemental Fig. S1).

k_{io} correlates with SUV. The correlation between the contrast kinetic parameters (including k_{io}) and SUV was assessed using a separate group of mice (n = 7) which had DCE-MRI scan immediately followed by FDG-PET. The 3D maps of contrast kinetic parameters and k_{io} have a relatively high spatial resolution that shows heterogeneous patterns of the tumor tissue, which cannot be appreciated in the SUV maps of FDG-PET with a lower spatial resolution (Fig. 4). The median values of the contrast kinetic parameters from the top ten percent enhancing voxels are compared with the mean SUV values (Fig. 5). The scatter plots in Fig. 5 show that

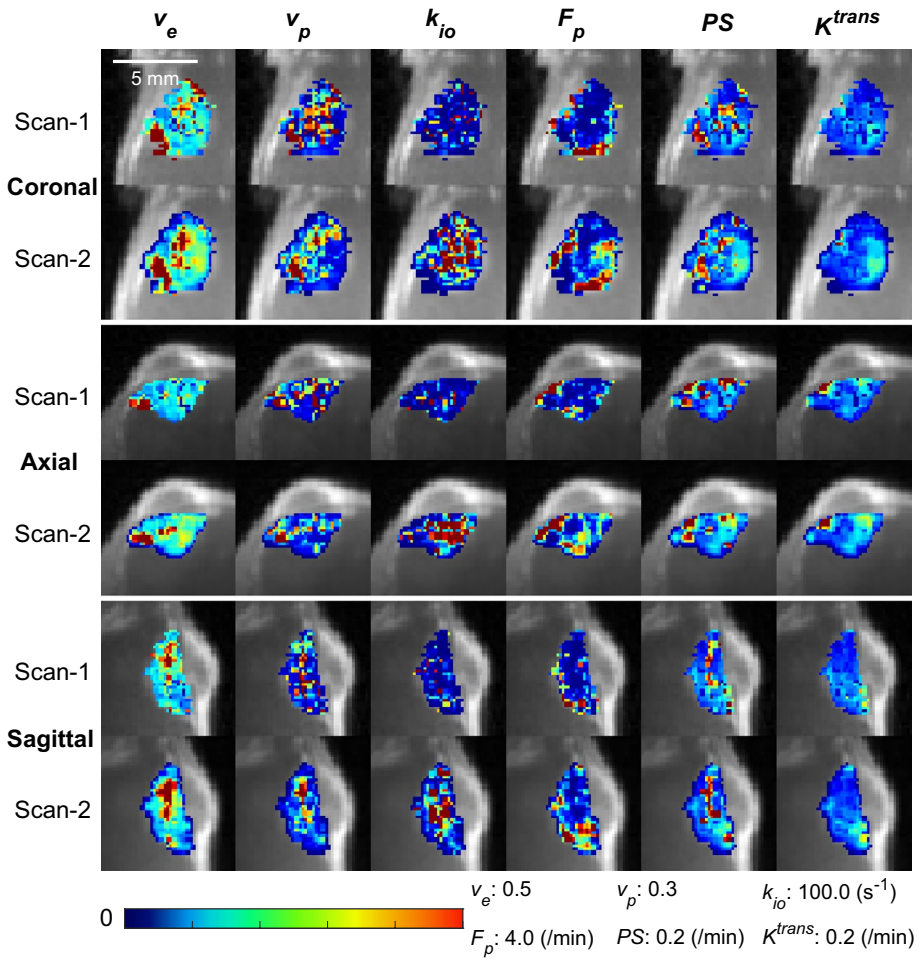

Figure 2. Contrast kinetic parameter and k_{io} maps of a GL261 tumor estimated using the 3D-UTE-GRASP DCE-MRI data acquired with the proposed two flip-angle method and an isotropic 3D resolution. This is a representative case from the test–retest study (n = 7) in which each mouse was scanned twice consecutively with an interval of 30 min. The whole tumor parameter maps of the Scan-2 are from the Scan-2 images registered to the Scan-1 images as shown in Fig. 1.

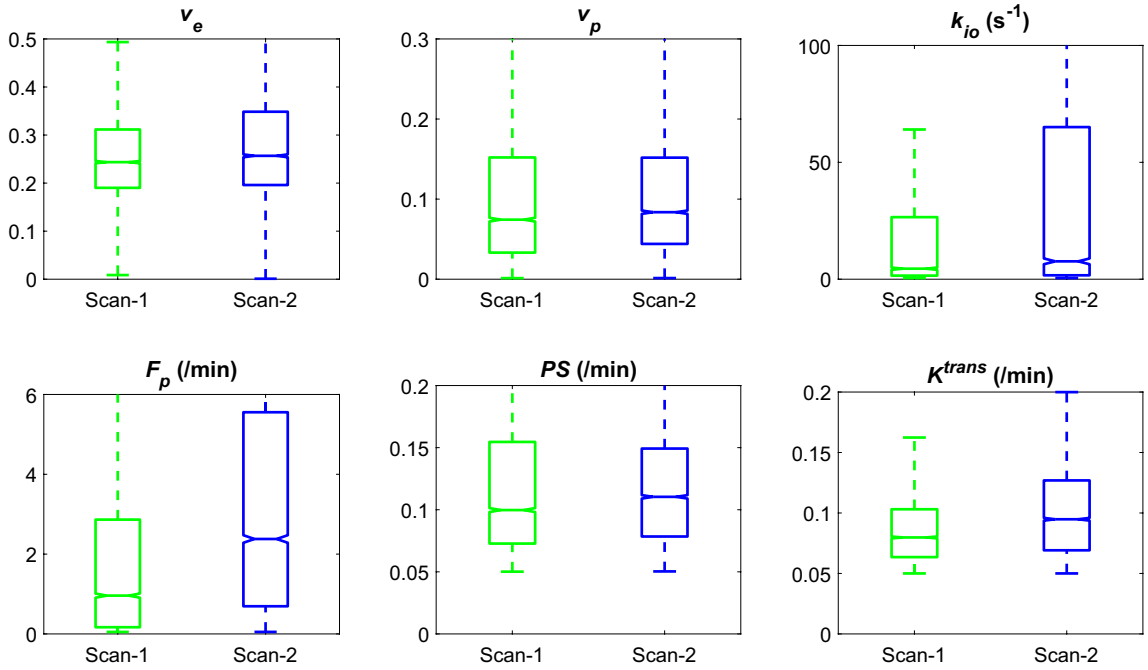

Figure 3. Comparison of whole tumor contrast kinetic parameters and k_{io} obtained from test–retest scans. All voxels in the tumors (n = 7) are pooled together for the box-whisker plots. There is no significant difference between the two scans in terms of the median values of parameters, except K^{trans} (P = 0.047). K^{trans} values were calculated from the F_p and PS values for individual voxels.

SUV has a positive correlation with k_{io} ($R^2 = 0.572$), k_{ex} ($R^2 = 0.547$), a positive correlation with F_p ($R^2 = 0.504$), and weak correlations with v_e ($R^2 = 0.150$), v_p ($R^2 = 0.077$), PS ($R^2 = 0.117$), K^{trans} ($R^2 = 0.088$) and whole tumor volume ($R^2 = 0.174$). Whole tumor SUV compared to whole tumor contrast kinetic parameter and k_{io} maps demonstrated strong correlations with PS ($R^2 = 0.693$) and K^{trans} ($R^2 = 0.651$) and weak correlations with all other parameters (Supplemental Fig. 2).

k_{io} is a sensitive marker for treatment response. The intracranial tumors in this study were growing aggressively; the tumors in both control and treated groups approximately tripled in volumes within the 4 days, from 3.10 ± 6.33 uL to 9.88 ± 26.73 uL, between the pre-treatment and Tx-2 (Figs. 6 and 7). While the volume did not show a significant difference between the control and treated groups at any time point, the k_{io} normalized to the baseline value showed a significant difference (P = 0.032) between the two groups at Tx-1. The normalized k_{io} and k_{ex} of the control group did not change significantly in the two imaging time points, while those of the treated group decreased significantly (P = 0.008 for both k_{io} and k_{ex}) at Tx-2. This pattern of change in k_{io} is observed more clearly in the tumor rims as shown in Fig. 6. The normalized v_e and v_p increased significantly (P = 0.008) between Pre-Tx and Tx-2 in both groups. In this study with a small number of animals, no significant difference between the two groups was observed in the contrast kinetic parameters and k_{io} without normalization to the baseline values (Table 1).

Discussion

Quantitative tissue microenvironment parameters measured from DCE-MRI may non-invasively capture the heterogenous properties of a tumor and their changes during tumor progresses and treatment. However, the adoption of these parameters in routine clinical imaging remains challenging and requires more work to establish the repeatability and reproducibility of the DCE-MRI data acquisition and analysis method[30]. Among the parameters of interest, the water efflux rate constant, k_{io}, is a unique parameter with potential as a biomarker for cellular energy turnover, but has proven difficult to measure[12,13]. The recently proposed method of using a multiple flip angle approach to actively encode the water exchange effect in the washout phase of the DCE-MRI scan, has demonstrated potential for improving the accuracy and precision of k_{io} estimation. In this present study, we further evaluated the multiple flip-angle method in terms of repeatability, correlation with SUV and sensitivity to treatment response.

We found that the compartmental volume fractions (v_e and v_p) remained consistent between the test and retest scans while the vascular functional measures (F_p and PS) and k_{io} showed noticeable changes, probably due to physiological changes of the tumor between the two scans. It is not trivial to measure repeatability of DCE-MRI parameters as the subject must fully clear the GBCA before a retest may be performed. On the other hand, aggressive tumors could have continuous changes in their volume and properties as observed in this study with GL261. For our study, hence, we performed a test–retest with a limited time interval of 30 min for GBCA to clear from the body as much as possible before repeating the DCE-MRI scan. We conducted T_1 mapping prior

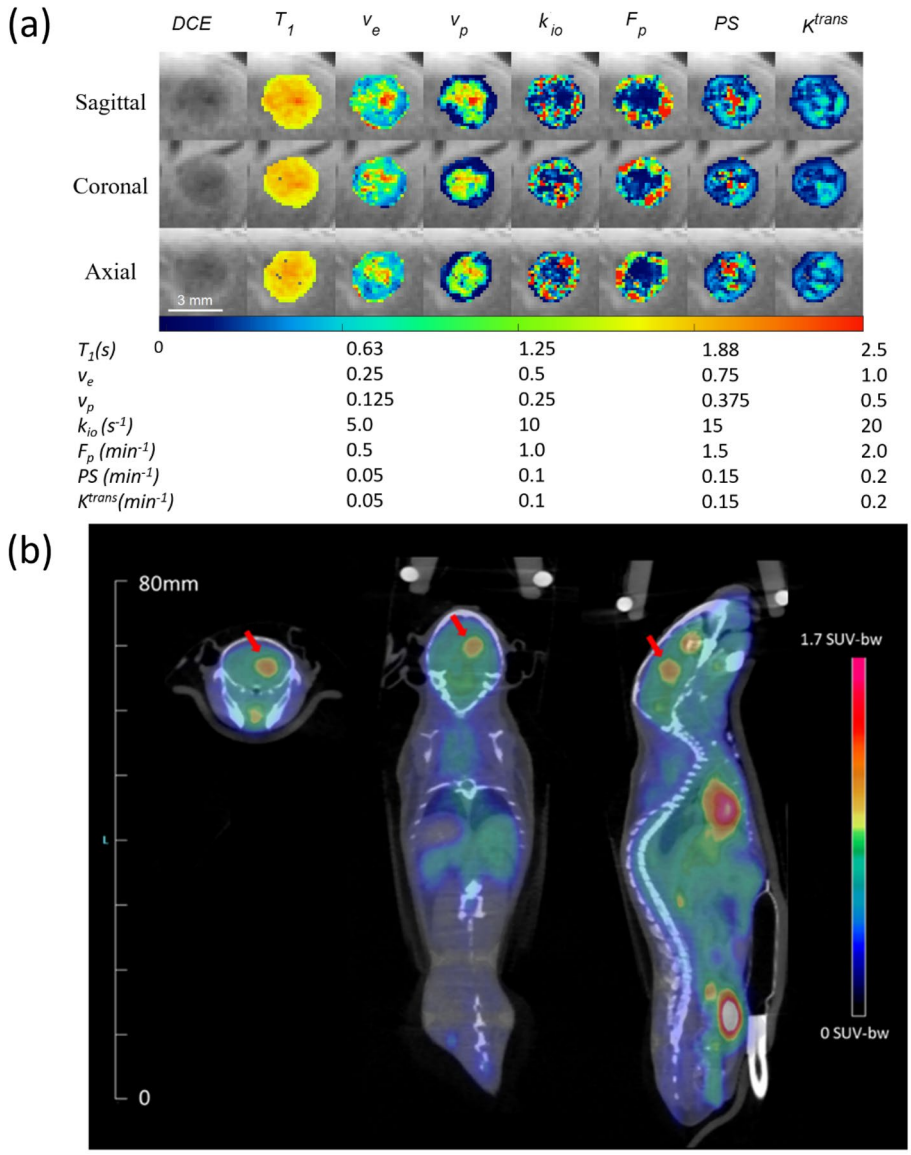

Figure 4. A representative case of a mouse with GL261 tumor scanned using DCE-MRI (**a**), immediately followed by ^{18}F-FDG-PET/CT (**b**). DCE-MRI scan was conducted using a high spatial resolution ($0.156 \times 0.156 \times 0.156$ mm^3) for the brain, whereas FDG-PET had a relatively lower spatial resolution ($1.4 \times 1.4 \times 1.4$ mm^3) covering the whole body. The heterogeneity of the tumor observed in DCE-MRI (**a**) is not clearly shown in the SUV map of the tumor (arrows) with a lower spatial resolution, overlaid on the CT image (**b**). The SUV map (**b**) was generated by the vendor software which may include some image processing for the display, whereas the DCE-MRI parameter maps (**a**) were shown without any interpolation or smoothing.

to each DCE-MRI scan such that the potential bias of remaining contrast agent in the tissue can be minimized in the contrast kinetic model analysis of the second data set.

Between the test and retest scans, we observed negligible changes in the estimated compartmental volume fraction parameters v_e and v_p. This is a reasonable outcome as we would not expect the cellular volumetric properties of the tumors to change substantially over the short duration of the experiment. In contrast, we observed noticeable increases in perfusion parameters (F_p, PS, and K^{trans}) and an increase in k_{io}. These changes from the first to the second scan may be explained by physiological changes induced by prolonged exposure to isoflurane altering blood flow in the mouse and tumor metabolism. Li et al.[31] demonstrated that cerebral blood flow in macaques increased in a dose dependent manner with isoflurane concentration. While isoflurane levels were maintained at low maintenance dosage (1–1.5% in air) throughout the experiment, prolonged exposure likely resulted in increased blood flow due to vasodilation. Furthermore, isoflurane has been shown to upregulate hypoxia-inducible factor 1-alpha (HIF1A) and vascular endothelial growth factor (VEGF) in cancer[32,33]. In vitro studies of ovarian cancer cells found that exposure to isoflurane increased angiogenesis, cell proliferation, and migration associated with increased levels of insulin-like growth factor 1 and VEGF[34]. One of the most prominent adaptations in hypoxic cells is increased glucose uptake and expression of glutamine transporters, to promote

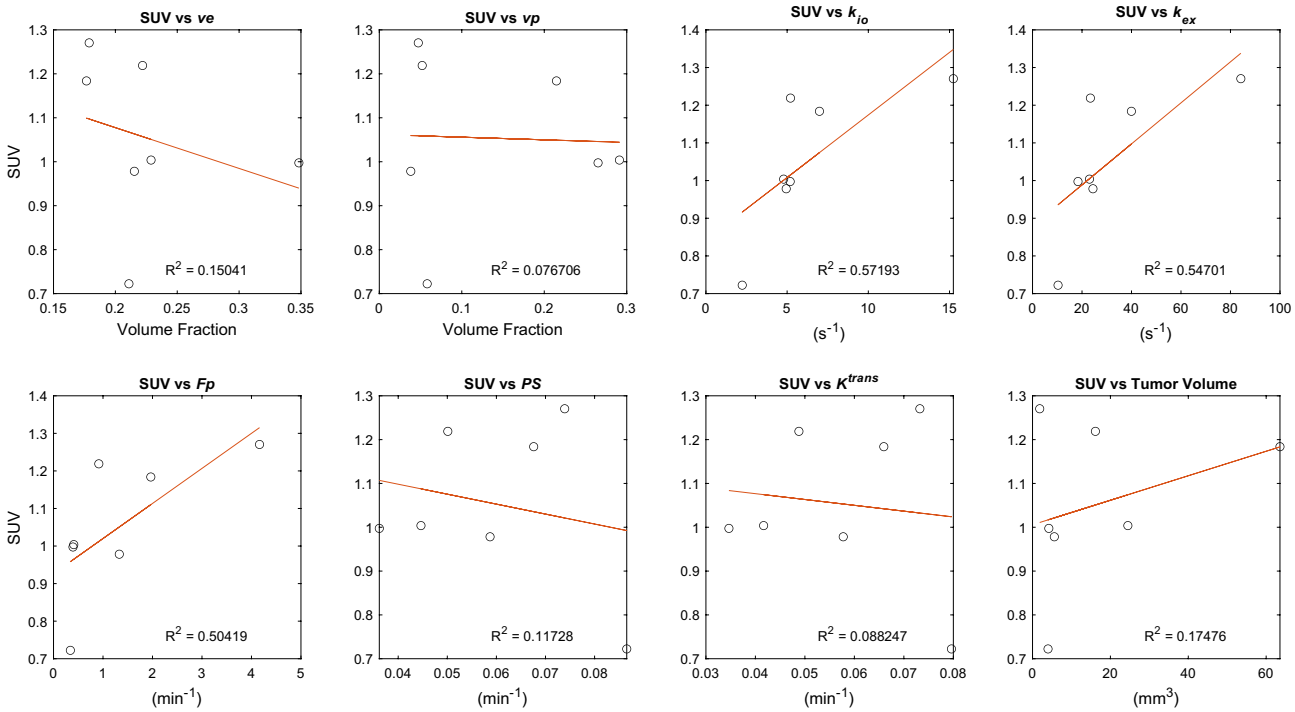

Figure 5. Scatter plots to assess the association between the contrast kinetic parameters and k_{io} estimated from top ten percent of enhancing voxels from DCE-MRI and whole tumor standardized uptake values (SUV) from FDG-PET. Data used in these plots are the median values of individual tumors (n = 7). The red lines are linear regression lines with the R^2 values shown in the plots.

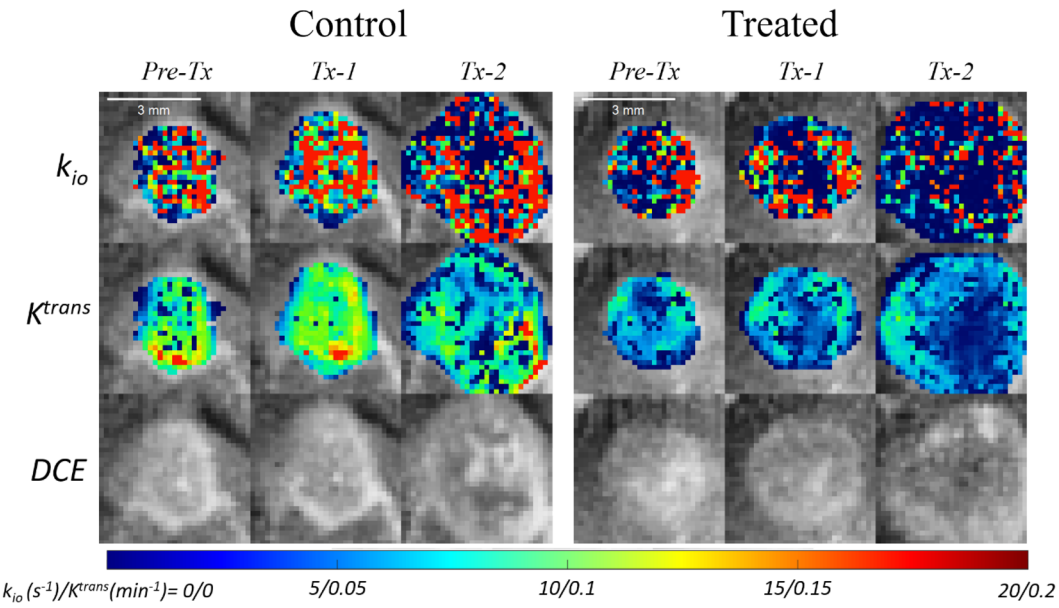

Figure 6. Representative k_{io} and K^{trans} parameter maps and the last frame of DCE-MR images of a mouse from the control group (left) and one from the treated group (right). The parameter maps are overlayed on the last frame of DCE-MR images (DCE). In both cases, it can be observed that the tumors grew aggressively within 4 days between Pre-tx and Tx-2.

glucose catabolism[35]. The increase in glucose metabolism would lead to an increase in water exchange, i.e. an increase in k_{io}. Hence, although the results of our study did not show a strong repeatability of k_{io}, they may suggest the sensitivity of k_{io} to the metabolic status of the cancer cells.

To better understand and probe the relationship of cellular water exchange with cellular metabolism, we compared k_{io} from DCE-MRI with SUV from ^{18}F-FDG-PET. SUV is widely used as a semi-quantitative measure

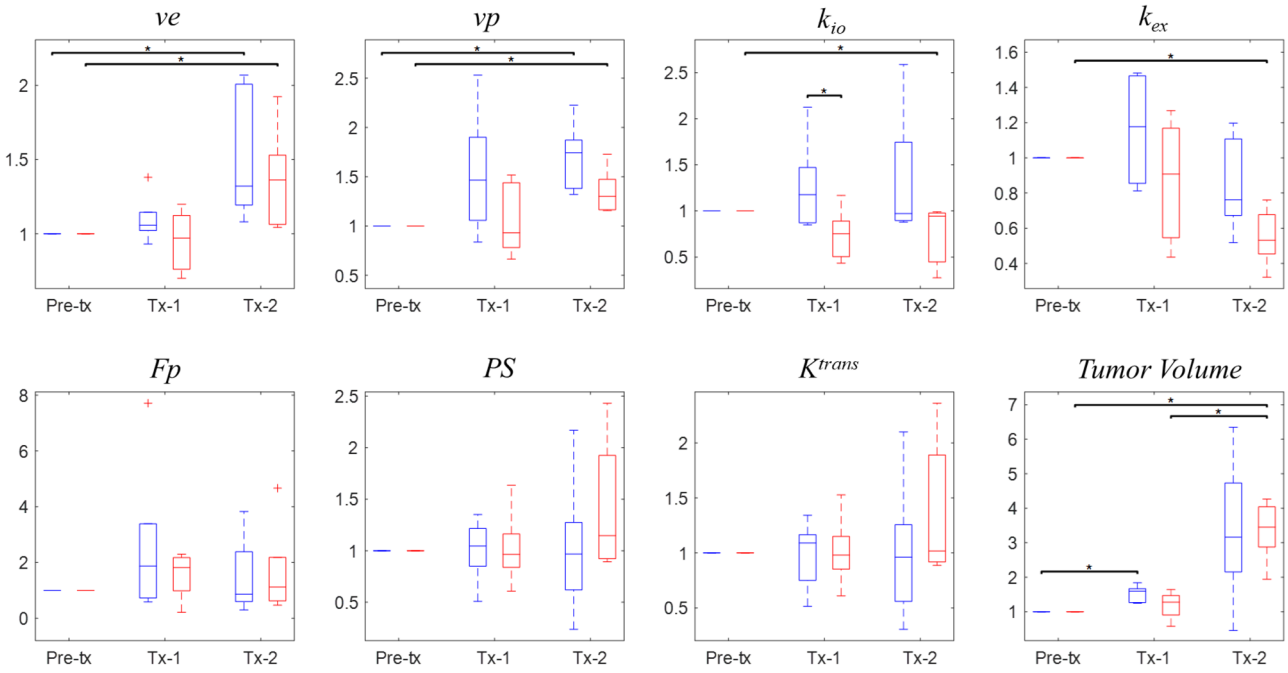

Figure 7. Normalized whole tumor contrast kinetic parameter and k_{io} median values for the control (blue, left) and treated (red, right) cohorts for pre-treatment (Pre-tx), 24 h post bevacizumab (Tx-1) and post two doses of fluorouracil (Tx-2) time points. Normalization was done by dividing each parameter by the Pre-tx values of the individual tumor. * denotes a statistical significance ($P < 0.05$) by the Wilcoxon rank sum test.

		v_e	v_p	k_{io} (s^{-1})	F_p (min^{-1})	PS (min^{-1})	K^{trans}(min^{-1})
Control	Pre-Tx	0.171 (0.091)	0.037 (0.082)	0.751 (3.970)	0.357 (0.826)	0.059 (0.068)	0.050 (0.050)
	Tx-1	0.180 (0.073)	0.042 (0.087)	1.335 (3.395)	0.694 (0.906)	0.069 (0.067)	0.049 (0.046)
	Tx-2	0.213 (0.074)	0.083 (0.130)	1.626 (3.020)	0.505 (0.333)	0.028 (0.035)	0.026 (0.029)
Treated	Pre-Tx	0.149 (0.050)	0.026 (0.022)	2.250 (1.600)	0.471 (1.057)	0.014 (0.017)	0.014 (0.014)
	Tx-1	0.120 (0.096)	0.025 (0.021)	1.251 (0.996)	0.586 (0.595)	0.014 (0.010)	0.013 (0.008)
	Tx-2	0.187 (0.062)	0.034 (0.030)	0.760 (0.486)	0.713 (0.787)	0.021 (0.016)	0.020 (0.012)

Table 1. Whole tumor contrast kinetic parameters and k_{io} (median (IQR)) measured at pre-treatment (Pre-tx), 24 h post bevacizumab (Tx-2) and post two doses of fluorouracil (Tx-2). The parameters normalized to the individual baseline values are shown in the plots of Fig. 7.

of glucose uptake and phosphorylation in tissue, an indicator of cellular metabolic activity. High SUV values are known to be associated with poor prognosis[36]. The correlation between k_{io} and SUV observed in this study further indicates k_{io} as a sensitive parameter for cellular metabolic activity. This observation is also in line with previous studies that showed the cellular water exchange is associated with Na + /K + ATPase activity and ATP-dependent ion channels in the plasma membrane[2,37,38]. The weak correlation between tumor volume and SUV suggests that the relationship between k_{io} and SUV is more likely driven by energy turnover than the bias of larger tumors acting as an FDG sink.

Several studies have demonstrated the feasibility of using k_{io} for monitoring and predicting tumor response to treatment and long term survivability[1,6,8,9,11]. Our present study explored the feasibility of using the multiple flip angle approach to estimate k_{io} during treatment of murine glioma using a combination therapy of bevacizumab, a monoclonal antibody against VEGF, and fluorouracil (5FU), a cytotoxic chemotherapeutic agent. Bevacizumab is often used in combination with other cytotoxic therapies as it could be used to normalize tumor vasculature, improving delivery of the secondary chemotherapeutic agent[39,40]. The effect of this drug combination appears to be captured well by our study, as we observed a decrease both in water exchange and v_p in the treated group, despite a persistent increase in tumor volume in both groups. Often, responding tumors do not demonstrate an immediate change in volume, or even grow after the first several treatments. This highlights the importance of biomarkers which may detect tumor response prior to volume reduction. Further study is warranted to establish these DCE-MRI measures as biomarkers to simultaneously measure the anti-angiogenic and cytotoxic effect of a combination therapy.

Limitations of our study includes small cohort sizes used in the individual experiments. While the statistical power is limited by the small cohort size, our study results demonstrate that the multiple flip angle method of

DCE-MRI can be used as a robust way to measure k_{io} in cancer imaging studies and can serve as the pilot data to design future studies with larger cohorts. The present study is also limited to single tumor model. Future studies can also include pathological measurements of transmembrane water channels as well as other proteins related to cellular metabolism, such as mitochondria pyruvate carrier, monocarboxylate transport, lactate dehydrogenase A, lactate dehydrogenase B and pyruvate dehydrogenase[41].

In this study, we found that contrast kinetic parameters and k_{io} of tumor can be estimated from a multiple flip-angle DCE-MRI data. We have demonstrated that k_{io} has a strong correlation with the SUV from ^{18}F-FDG PET, suggesting the feasibility of using k_{io} as an imaging marker for cellular metabolic activity without using a radioactive contrast agent. The results of this study also support the potential of k_{io} to discern tumors responding to a vascular normalization treatment and cytotoxic chemotherapeutics. Further study with a larger cohort is warranted to establish the cellular water exchange in cancer metabolism and its changes during progression and treatment.

Data availability

The datasets used and/or analyzed during the current study available from the corresponding author on reasonable request.

Received: 1 July 2022; Accepted: 14 February 2023
Published online: 21 February 2023

References

1. Springer, C. S. *et al.* Intratumor mapping of intracellular water lifetime: Metabolic images of breast cancer?. *NMR Biomed.* **27**(7), 760–773. https://doi.org/10.1002/nbm.3111 (2014).
2. Zhang, Y., Poirier-Quinot, M., Springer, C. S. & Balschi, J. A. Active trans-plasma membrane water cycling in yeast is revealed by NMR. *Biophys. J.* **101**(11), 2833. https://doi.org/10.1016/J.BPJ.2011.10.035 (2011).
3. Loo, D. D. F., Zeuthen, T., Chandy, G. & Wright, E. M. Cotransport of water by the Na+/glucose cotransporter. *Proc. Natl. Acad. Sci. U. S. A.* **93**(23), 13367–13370. https://doi.org/10.1073/PNAS.93.23.13367 (1996).
4. Ribatti, D., Ranieri, G., Annese, T. & Nico, B. Aquaporins in cancer. *Biochim. Biophys. Acta* **1840**(5), 1550–1553. https://doi.org/10.1016/j.bbagen.2013.09.025 (2014).
5. Bai, R. *et al.* Shutter-speed DCE-MRI analyses of human glioblastoma multiforme (GBM) data. *J. Magn. Reson. Imaging* **52**(3), 850–863. https://doi.org/10.1002/JMRI.27118 (2020).
6. Lowry, M. *et al.* Analysis of prostate DCE-MRI: Comparison of fast exchange limit and fast exchange regimen pharmacokinetic models in the discrimination of malignant from normal tissue. *Invest. Radiol.* **44**(9), 577–584. https://doi.org/10.1097/RLI.0B013E3181B4C1FE (2009).
7. Li, X. *et al.* Cell membrane water exchange effects in prostate DCE-MRI. *J. Magn. Reson.* **218**, 77–85. https://doi.org/10.1016/J.JMR.2012.03.019 (2012).
8. Kim, S. *et al.* Prediction of response to chemoradiation therapy in squamous cell carcinomas of the head and neck using dynamic contrast-enhanced MR imaging. *AJNR Am. J. Neuroradiol.* **31**(2), 262–268. https://doi.org/10.3174/AJNR.A1817 (2010).
9. Tudorica, A. *et al.* Early prediction and evaluation of breast cancer response to neoadjuvant chemotherapy using quantitative DCE-MRI. *Transl. Oncol.* **9**(1), 8–17. https://doi.org/10.1016/J.TRANON.2015.11.016 (2016).
10. Do, R. K. *et al.* Diffusion-weighted and dynamic contrast-enhanced MRI derived imaging metrics for stereotactic body radiotherapy of pancreatic ductal adenocarcinoma: Preliminary findings. *Tomography.* **6**(2), 261. https://doi.org/10.18383/J.TOM.2020.00015 (2020).
11. Chawla, S. *et al.* Dynamic contrast-enhanced MRI-derived intracellular water lifetime (T i): A prognostic marker for patients with head and neck squamous cell carcinomas. *Am. J. Neuroradiol.* **39**(1), 138–144. https://doi.org/10.3174/ajnr.A5440 (2018).
12. Zhang, J. & Kim, S. Uncertainty in MR tracer kinetic parameters and water exchange rates estimated from T1-weighted dynamic contrast enhanced MRI. *Magn. Reson. Med.* **72**(2), 534–545. https://doi.org/10.1002/MRM.24927/ASSET/SUPINFO/MRM24927-SUP-0003-SUPPINFO.TIF (2014).
13. Buckley, D. L. Shutter-speed dynamic contrast-enhanced MRI: Is it fit for purpose?. *Magn. Reson. Med.* **81**(2), 976–988. https://doi.org/10.1002/MRM.27456 (2019).
14. Bains, L. J. *et al.* Tracer kinetic analysis of dynamic contrast-enhanced MRI and CT bladder cancer data: A preliminary comparison to assess the magnitude of water exchange effects. *Magn. Reson. Med.* **64**(2), 595–603. https://doi.org/10.1002/MRM.22430 (2010).
15. Spencer, R. G. S. & Fishbein, K. W. Measurement of spin-lattice relaxation times and concentrations in systems with chemical exchange using the one-pulse sequence: Breakdown of the Ernst model for partial saturation in nuclear magnetic resonance spectroscopy. *J. Magn. Reson.* **142**(1), 120–135. https://doi.org/10.1006/JMRE.1999.1925 (2000).
16. Zhang, J. & Kim, S. G. Estimation of cellular-interstitial water exchange in dynamic contrast enhanced MRI using two flip angles. *NMR Biomed.* **32**(11), 1–17. https://doi.org/10.1002/nbm.4135 (2019).
17. Zhang, J., Feng, L., Otazo, R. & Kim, S. G. Rapid dynamic contrast-enhanced MRI for small animals at 7T using 3D ultra-short echo time and golden-angle radial sparse parallel MRI. *Magn. Reson. Med.* **81**(1), 140–152. https://doi.org/10.1002/mrm.27357 (2019).
18. Zhang, J., Winters, K., Reynaud, O. & Kim, S. G. Simultaneous measurement of T1/B1 and pharmacokinetic model parameters using active contrast encoding (ACE)-MRI. *NMR Biomed.* **30**(9), e3737. https://doi.org/10.1002/nbm.3737 (2017).
19. Brix, G. *et al.* Microcirculation and microvasculature in breast tumors: Pharmacokinetic analysis of dynamic MR image series. *Magn. Reson. Med.* **52**(2), 420–429. https://doi.org/10.1002/MRM.20161 (2004).
20. Li, X., Rooney, W. D. & Springer, C. S. A unified magnetic resonance imaging pharmacokinetic theory: Intravascular and extracellular contrast reagents. *Magn. Reson. Med.* **54**(6), 1351–1359. https://doi.org/10.1002/MRM.20684 (2005).
21. McConnell, H. M. Reaction rates by nuclear magnetic resonance. *J. Chem. Phys.* **28**(3), 430–431. https://doi.org/10.1063/1.1744152 (1958).
22. Jensen, J. H. & Helpern, J. A. Effect of gradient pulse duration on MRI estimation of the diffusional kurtosis for a two-compartment exchange model. *J. Magn. Reson.* **210**(2), 233. https://doi.org/10.1016/J.JMR.2011.03.012 (2011).
23. Fieremans, E., Novikov, D. S., Jensen, J. H. & Helpern, J. A. Monte Carlo study of a two-compartment exchange model of diffusion. *NMR Biomed.* **23**(7), 711–724. https://doi.org/10.1002/NBM.1577 (2010).
24. Zhang, J. *et al.* Measurement of cellular-interstitial water exchange time in tumors based on diffusion-time-dependent diffusional kurtosis imaging. *NMR Biomed.* **34**(6), e4496. https://doi.org/10.1002/NBM.4496 (2021).
25. Van Griethuysen, J. J. M. *et al.* Computational radiomics system to decode the radiographic phenotype. *Cancer Res.* **77**(21), e104–e107. https://doi.org/10.1158/0008-5472.CAN-17-0339 (2017).

26. Freedman, D. & Diaconis, P. On the histogram as a density estimator:L2 theory. *Zeitschrift für Wahrscheinlichkeitstheorie und Verwandte Gebiete* **57**(4), 453–476. https://doi.org/10.1007/BF01025868 (1981).
27. Landis, C. S. *et al.* Equilibrium transcytolemmal water-exchange kinetics in skeletal muscle in vivo. *Magn. Reson. Med.* **42**(3), 467–478. https://doi.org/10.1002/(SICI)1522-2594(199909)42:3%3c467::AID-MRM9%3e3.0.CO;2-0 (1999).
28. Sourbron, S. P. & Buckley, D. L. Tracer kinetic modelling in MRI: Estimating perfusion and capillary permeability. *Phys. Med. Biol.* **57**(2), R1–R33. https://doi.org/10.1088/0031-9155/57/2/R1 (2012).
29. Buckley, D. L., Kershaw, L. E. & Stanisz, G. J. Cellular-interstitial water exchange and its effect on the determination of contrast agent concentration in vivo: Dynamic contrast-enhanced MRI of human internal obturator muscle. *Magn. Reson. Med.* **60**(5), 1011–1019. https://doi.org/10.1002/MRM.21748 (2008).
30. Shukla-Dave, A. *et al.* Quantitative imaging biomarkers alliance (QIBA) recommendations for improved precision of DWI and DCE-MRI derived biomarkers in multicenter oncology trials. *J. Magn. Reson. Imaging* **49**(7), e101–e121. https://doi.org/10.1002/jmri.26518 (2019).
31. Li, C. X., Patel, S., Wang, D. J. J. & Zhang, X. Effect of high dose isoflurane on cerebral blood flow in macaque monkeys. *Magn. Reson. Imaging* **32**(7), 956. https://doi.org/10.1016/J.MRI.2014.04.019 (2014).
32. Huang, H. *et al.* Prostate cancer cell malignancy via modulation of HIF-1α pathway with isoflurane and propofol alone and in combination. *Br. J. Cancer* **111**(7), 1338–1349. https://doi.org/10.1038/BJC.2014.426 (2014).
33. Benzonana, L. L. *et al.* Isoflurane, a commonly used volatile anesthetic, enhances renal cancer growth and malignant potential via the hypoxia-inducible factor cellular signaling pathway in vitro. *Anesthesiology* **119**(3), 593–605. https://doi.org/10.1097/ALN.0B013E31829E47FD (2013).
34. Luo, X. *et al.* Impact of isoflurane on malignant capability of ovarian cancer in vitro. *Br. J. Anaesth.* **114**(5), 831–839. https://doi.org/10.1093/BJA/AEU408 (2015).
35. Lee, P., Chandel, N. S. & Simon, M. C. Cellular adaptation to hypoxia through HIFs andbeyond. *Nat. Rev. Mol. Cell. Biol.* **21**(5), 268. https://doi.org/10.1038/S41580-020-0227-Y (2020).
36. Lucignani, G., Paganelli, G. & Bombardieri, E. The use of standardized uptake values for assessing FDG uptake with PET in oncology: A clinical perspective. *Nucl. Med. Commun.* **25**(7), 651–656. https://doi.org/10.1097/01.MNM.0000134329.30912.49 (2004).
37. Ruggiero, M. R. *et al.* Evidence for the role of intracellular water lifetime as a tumour biomarker obtained by in vivo field-cycling relaxometry. *Angew Chem. Int. Ed. Engl.* **57**(25), 7468–7472. https://doi.org/10.1002/ANIE.201713318 (2018).
38. Bai, R., Springer, C. S., Plenz, D. & Basser, P. J. Fast, Na+/K+ pump driven, steady-state transcytolemmal water exchange in neuronal tissue: A study of rat brain cortical cultures. *Magn. Reson. Med.* **79**(6), 3207–3217. https://doi.org/10.1002/mrm.26980 (2018).
39. Presta LG, Chen H, O'Connor SJ, et al. Humanization of an anti-vascular endothelial growth factor monoclonal antibody for the therapy of solid tumors and other disorders. *Cancer Res.* 1997;57(20):4593–4599. https://pubmed.ncbi.nlm.nih.gov/9377574/ Accessed on 20 December 2021.
40. Hurwitz, H. *et al.* Bevacizumab plus irinotecan, fluorouracil, and leucovorin for metastatic colorectal cancer. *N. Engl. J. Med.* **350**(23), 2335–2342. https://doi.org/10.1056/NEJMOA032691 (2004).
41. Ruiz-Iglesias, A. & Mañes, S. The importance of mitochondrial pyruvate carrier in cancer cell metabolism and tumorigenesis. *Cancers (Basel)* **13**(7), 1488. https://doi.org/10.3390/CANCERS13071488 (2021).

Acknowledgements

We thank Zakia Gironda and Orin Mishkit of the NYU Preclinical Imaging Core for their expertise and assistance with the ^{18}F-FDG PET study. This work was partially supported by NIH/NCI grants R01CA160620, R01CA219964, and UG3CA22869, as well as the NSF-DMREF (DMR 1728858) and the NYU Shiffrin-Myers Breast Cancer Discovery Fund. The NYU Preclinical Imaging Core is partially supported by NIH grants 5P30CA016087 and P41 EB017183.

Author contributions

K.K. and G.K. wrote the main manuscript text. J.Z. prepared Figs. 1, 2 and 3 and K.K. prepared Figs. 4, 5, 6 and 7. A.D. and J.T. collected data for 'Repeatability' experiment and J.Z performed analysis. K.K. collected data and performed analysis for 'Comparison of DCE-MRI with FDG-PET' and 'Assessment of Treatment Response' experiments. All authors reviewed the manuscript.

Competing interests

The authors declare no competing interests.

Additional information

Supplementary Information The online version contains supplementary material available at https://doi.org/10.1038/s41598-023-29991-1.

Correspondence and requests for materials should be addressed to K.K.

Reprints and permissions information is available at www.nature.com/reprints.

Publisher's note Springer Nature remains neutral with regard to jurisdictional claims in published maps and institutional affiliations.